Laurson, L.; Durin, G.; Zapperi, S.

Universality classes and crossover scaling of Barkhausen noise in thin films

Universality classes and crossover scaling of Barkhausen noise in thin films

Lasse Laurson,[1] Gianfranco Durin,[2,3] and Stefano Zapperi[2,4]

[1]*COMP Centre of Excellence and Helsinki Institute of Physics, Department of Applied Physics, Aalto University, P.O. Box 11100, FIN-00076 Aalto, Espoo, Finland*

[2]*ISI Foundation, Via Alassio 11/c 10126 Torino, Italy*

[3]*Istituto Nazionale di Ricerca Metrologica, strada delle Cacce 91, 10135 Torino, Italy*

[4]*CNR - Consiglio Nazionale delle Ricerche, IENI, Via R. Cozzi 53, 20125 Milano, Italy*

We study the dynamics of head-to-head domain walls separating in-plane domains in a disordered ferromagnetic thin film. The competition between the domain-wall surface tension and dipolar interactions induces a crossover between a rough domain-wall phase at short length scales and a large-scale phase where the walls display a zigzag morphology. The two phases are characterized by different critical exponents for Barkhausen avalanche dynamics that are in quantitative agreement with experimental measurements on MnAs thin films.

I. INTRODUCTION

When subject to an external magnetic field, a ferromagnetic material shows a sequence of discrete and intermittent jumps of the magnetic domain walls (DW's), known as the Barkhausen effect [1], a paradigmatic example of crackling noise in materials [2]. The statistical properties of the Barkhausen noise are usually studied by measuring the size distribution $P(s)$ of such jumps, or avalanches, which typically follows a power law $P(s) \sim s^{-\tau}$, with the exponent τ characterizing the universality class of the avalanche dynamics. In three-dimensional bulk ferromagnetic materials, the scaling behavior of the Barkhausen effect is understood theoretically in terms of the depinning transition of domain walls [3] with two distinct universality classes for amorphous and polycrystalline materials [4]. A similar clear-cut classification does not exist in lower dimensions, despite Barkhausen avalanches having been studied experimentally for decades in several ferromagnetic thin films with in-plane [5–10] or out-of-plane anisotropy [11,12]. This issue is particularly important because these low-dimensional magnetic structures have become increasingly relevant for various technological applications [13,14].

An important step towards understanding the different universality classes in thin films was achieved by the magneto-optical experiments of Ryu *et al.* [10], who observed a crossover between two different avalanche size exponents τ as temperature T was varied close to but below the Curie temperature T_c of a 50-nm MnAs film. This crossover was accompanied by changes in DW morphology, such that the DW structure evolves from rough for high T to DW's with a pronounced tendency to form zigzag or sawtoothlike patterns for lower T. It was argued that by varying T close to T_c, one can tune the value of the squared saturation magnetization M_s^2, and thus the strength of the long-range dipolar interactions between different DW segments. The zigzag pattern is expected to arise as a result of a competition between the domain-wall energy and the dipolar interactions, with the former favoring a flat horizontal DW, while the latter would prefer a vertically spread DW to reduce the magnetic charge density [15–19].

In this paper, we provide a theoretical explanation of the experimentally observed universality classes and the crossover between them. Starting from micromagnetic theory, we derive

an equation of motion for a line model of a head-to-head DW in a two-dimensional thin film separating in-plane domains. By numerical simulations and theoretical analysis, we show that the model exhibits a crossover between two universality classes of the Barkhausen avalanche dynamics, resulting from a competition between DW surface tension and dipolar interactions. We present a detailed characterization of the DW morphology, avalanche dynamics, and the crossover scaling between the two universality classes. The paper is organized as follows: In the next section (Sec. II), we derive the line model of the head-to-head DW, and study it numerically and theoretically in Sec. III. Finally, Sec. IV finishes the paper with discussion and conclusions.

II. MODEL

Due to the essentially two-dimensional thin-film geometry considered here (the film thickness Δ_z is much smaller than the DW length), we model the DW as a flexible line Σ with surface tension γ_w due to DW energy. The line moves within the xy plane, and has an average orientation along the x axis. It is taken to separate two magnetic domains with magnetization along $\pm\hat{\mathbf{y}}$, respectively. Thus, a head-to-head DW is characterized by a magnetic charge density $\sigma(\mathbf{r}) = 2M_s \cos\theta(\mathbf{r})$ along the DW, with $\theta(\mathbf{r})$ the angle between the local DW normal $\hat{\mathbf{n}}$ and the $\hat{\mathbf{y}}$ direction. These magnetic charges then lead to a magnetostatic field $\mathbf{H}_m(\mathbf{r}) = \int_{\Sigma'} \sigma(\mathbf{r}')(\mathbf{r} - \mathbf{r}')/|\mathbf{r} - \mathbf{r}'|^3 ds'$, the y component of which produces a normal pressure acting on the DW segments, along with an applied field $\mathbf{H}_a = H_a\hat{\mathbf{y}}$. In addition, the DW segments interact with quenched disorder, described by a random pressure field $\eta(\mathbf{r})$ due to short-range interactions with random pinning centers. Thus, the total normal pressure difference Δp acting across the DW at point $\mathbf{r}$ reads

$$\Delta p(\mathbf{r}) = \gamma_w / R(\mathbf{r}) + 2M_s \mu_0 H_a + \eta(\mathbf{r}) \cdot \hat{\mathbf{n}}$$
$$+ 4\mu_0 M_s^2 \int_{\Sigma(\mathbf{r}')} \frac{(y - y')\cos\theta'}{[(x - x')^2 + (y - y')^2]^{3/2}} ds', \quad (1)$$

where $R(\mathbf{r})$ is the local radius of curvature. To simulate such a system, we discretize the DW along the x direction, by using the film thickness Δ_z as the lattice constant, and describe the

DW by a single-valued function $y = h(x,t)$ (implying that formation of overhangs are excluded by construction), with $x = i = 1,2,\ldots,L$. The local DW velocity is assumed to be proportional to the local pressure acting on the DW, such that the equation of motion for the DW line segment i along the y direction is given by

$$\Gamma \frac{\partial h_i}{\partial t} = \frac{1}{\cos \theta_i} \left[\gamma_w \frac{\partial^2 h_i}{\partial x^2} + 2M_s \mu_0 H_a + \eta(i,h_i) \right.$$

$$\left. + 4\mu_0 M_s^2 \Delta_z^2 \sum_{j \neq i} \frac{h_i - h_j}{\left[\Delta_z^2 (i-j)^2 + (h_i - h_j)^2 \right]^{3/2}} \right],$$

$$(2)$$

where we have approximated the curvature term by a discretized Laplacian, θ_i is the angle between the normal of the ith segment and the y direction, and Γ is a damping constant. The factor $1/\cos\theta_i$ multiplying the right-hand side of Eq. (2) transforms normal motion into motion along the y direction. The quenched random force has correlations $\langle \eta(i,h_i)\eta(j,h_j)\rangle = \sigma^2 \delta(i-j)\delta(h_i - h_j)$. We further write Eq. (2) in nondimensional units, by measuring lengths in units of Δ_z and times in units of $\Gamma \Delta_z/(\mu_0 M_s^2)$. The resulting dimensionless equation of motion reads

$$\frac{\partial h_i}{\partial t} = \frac{1}{\cos \theta_i} \left[\lambda \frac{\partial^2 h_i}{\partial x^2} + F_{\text{ext}} + \eta(i,h_i) \right.$$

$$\left. + 4 \sum_{j \neq i} \frac{h_i - h_j}{[(i-j)^2 + (h_i - h_j)^2]^{3/2}} \right], \qquad (3)$$

where the dimensionless driving force is $F_{\text{ext}} = 2H_a/M_s$ and $\lambda \equiv l_D/\Delta_z$ is the ratio between the "domain formation" length [20] $l_D = \gamma_w/(\mu_0 M_s^2)$ and the film thickness. In dimensionless units, the quenched random force has correlations $\langle \eta(i,h_i)\eta(j,h_j)\rangle = \sigma_{nd}^2 \delta(i-j)\delta(h_i - h_j)$, with $\sigma_{nd} = \sigma/(\mu_0 M_s^2 \Delta_z)$. Periodic boundary conditions are implemented by using the nearest image approximation to compute the nonlocal dipolar forces. Notice that the dipolar interaction term in Eq. (3) acts like a negative surface tension, i.e., it is nonconvex. Thus, some typical properties of elastic interfaces in random media, such as the no-passing rule [21], are not expected to hold.

III. RESULTS

To mimic the experiments of Ruy *et al.* [10], we simulate the system by integrating Eq. (3) numerically for a lateral system size $L = 512$, fixing the external force F_{ext} to a constant value below the critical depinning force F_c (above which the DW would keep moving continuously with a nonzero time-averaged velocity), and monitor the dynamics of the DW. The results are averaged over several realizations of the random impurity configuration. Whenever the average DW velocity $V(t) = 1/L \sum_i \partial h_i/\partial t$ falls below a low threshold value V_{th}, a randomly selected DW segment is given a "kick," such that an additional local force acting on the DW segment is first increased linearly from zero until $V > V_{\text{th}}$, and then decreased continuously back to zero. This can then trigger
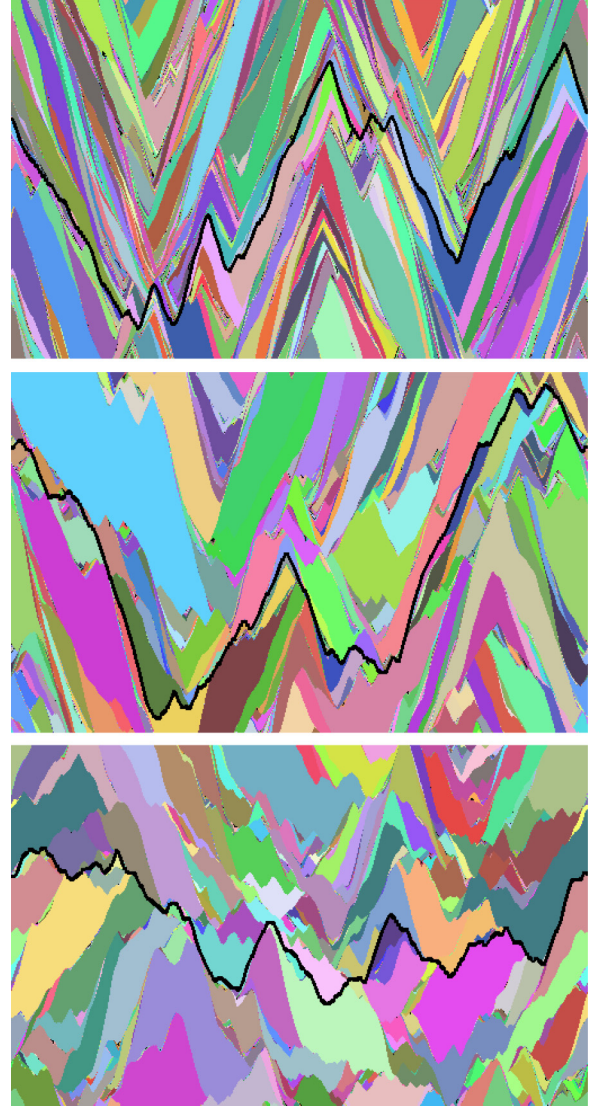

FIG. 1. (Color online) The spatial structure of Barkhausen avalanches for $\lambda = 1$ (top), $\lambda = 2$ (middle), and $\lambda = 4$ (bottom). The domain wall is moving from top to bottom, and the area swept over by each avalanche has been colored with a random color. An example of the DW structure is given by a black line in each case.

an avalanche, which lasts until the average velocity of the front again falls below V_{th}, and the process is repeated. The area (measured in units of Δ_z^2) over which the DW moves between two such triggering events (which mimic the effect of thermal activation) is taken to be the avalanche size s. Figure 1 shows typical examples of the spatial structure of the avalanches for different λ values. Note that tuning λ in the model corresponds to varying temperature in an experiment, which close to the Curie temperature affects the value of M_s, and consequently the strength of the dipolar interactions [10]. For small λ, the DW's exhibit a clear zigzag morphology (with avalanches tilted accordingly), and roughen due to disorder as λ is increased.

We further characterize the zigzag morphology by considering the distributions of the local slopes $\partial h/\partial x$ of the DW; see Fig. 2. For finite λ, the distributions are bimodal, reflecting
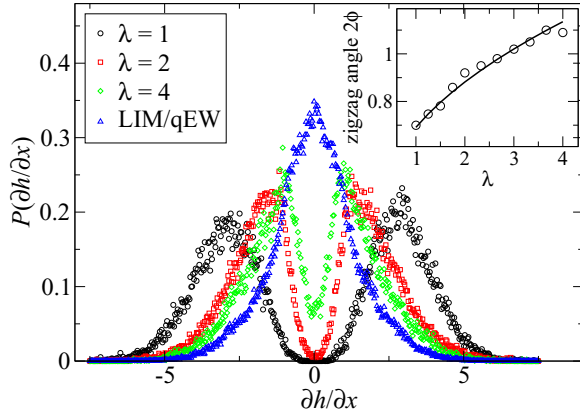
FIG. 2. (Color online) Distributions of the local slopes $\partial h/\partial x$ (see text for definition) for various λ. The inset shows the corresponding zigzag angle 2ϕ as a function of λ. The solid line is a fit to of Eq. (5), corresponding to $l = 3.9$.

the fact that the dipolar interactions render the flat DW unstable. For the sake of comparison, we show also the slope distribution for the linear interface model (LIM)/quenched Edwards-Wilkinson (qEW) equation [i.e., Eq. (3) without the nonlocal term, corresponding to the limit $\lambda \to \infty$], displaying a single peak at $\partial h/\partial x = 0$. The inset of Fig. 2 shows the zigzag angle 2ϕ, defined as $2\phi = 2\tan^{-1}(1/\langle|\partial h/\partial x|\rangle)$. For small $\lambda \sim 1/M_s^2$, 2ϕ is linear in λ, similar to experimental results [22], while for very large λ the DW becomes rough (i.e., the DW morphology is given by the usual roughness properties of the LIM/qEW case), and the concept of the zigzag angle is ill-defined. An approximate analytical estimate of the λ dependence of 2ϕ can be obtained by requiring balance between forces due to line tension and dipolar interactions. The former can be estimated as $\lambda\partial^2 h/\partial x^2 = \lambda 2m/l$, where $m = \langle|\partial h/\partial x|\rangle$ is the average magnitude of the local zigzag slope, and l is the length of the "transition region" at the tip of the zigzag where a constant curvature $2m/l$ is assumed. These have to be balanced by forces due to dipolar interactions, which we write in terms of the slope m as

$$4\sum_{j\neq i} \frac{m|i-j|}{|i-j|^3(1+m^2)^{3/2}} = 4\frac{m}{(1+m^2)^{3/2}}2\zeta(2), \quad (4)$$

where $\zeta(2) = \pi^2/6$. Thus, from the force balance condition, one obtains for the slope $m = \sqrt{(2\pi^2 l/3\lambda)^{2/3} - 1}$, corresponding to the zigzag angle

$$2\phi = 2\tan^{-1}(m^{-1}) = 2\tan^{-1}[(2\pi^2 l/3\lambda)^{2/3} - 1]^{-1/2}. \quad (5)$$

A good fit to the data with Eq. (5) can be obtained by using l as a fitting parameter, resulting in $l \approx 3.9$; see the inset of Fig. 2.

We also quantify the morphology of the DWs by considering the roughness exponent ζ of the fronts. To this end, we compute the power spectrum $S(k)$ of the line profiles $h(x)$, expected to scale as $S(k) \propto k^{-(2\zeta+1)}$. Figure 3 shows $S(k)$ of the $\lambda = 1$ case, resulting in $\zeta \approx 1.5$: Thus, when a dipolar interaction term, favoring vertical spread of the DW, is added to the LIM/qEW model with $\zeta \approx 1.25$ [23], the fronts become more rough. In Fig. 3, we also consider a slope-subtracted
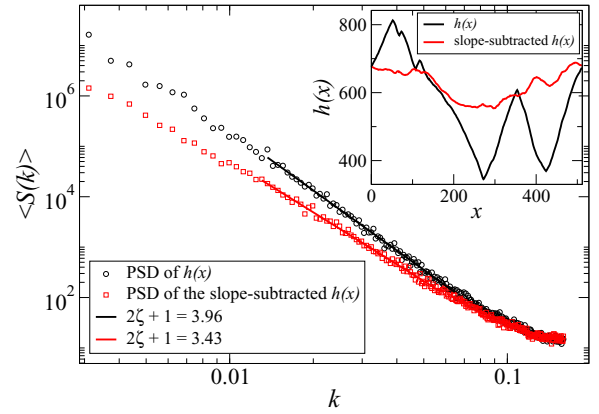

FIG. 3. (Color online) Main figure: Power spectra $S(k)$ of the DW profile $h(x)$ and of the slope-subtracted $h(x)$ for $\lambda = 1$, exhibiting scaling of the form of $S(k) \propto k^{-(2\zeta+1)}$, with ζ the roughness exponent. Inset shows examples of $h(x)$ and the corresponding slope-subtracted front, from which the average local tilt (the zigzag slope m) has been subtracted.

version of the $\lambda = 1$ fronts (see the inset of Fig. 3), where the average local zigzag slope (positive or negative depending on the DW segment) has been subtracted from $h(x)$. The power spectrum of the resulting fronts is characterized by $\zeta \approx 1.25$, i.e., it is indistinguishable from the LIM/qEW result. Thus, it seems that dipolar interactions induce a local tilt (the zigzag slope) to the otherwise LIM/qEW-like fronts.

For small λ, the statistical properties of the Barkhausen avalanches are expected to reflect the dominant nature of the dipolar interactions. Figure 4 shows the avalanche size distributions $P(s)$ for $\lambda = 1$ and various $F_{ext} < F_c$. By fitting the data using the least-squares method [24], the distributions are found to obey

$$P(s) = s^{-\tau_{DIP}}\mathcal{F}_{DIP}\left[\frac{s}{(F_c - F_{ext})^{-1/\sigma_{DIP}}}\right], \quad (6)$$

where $\mathcal{F}_{DIP}(x)$ is a scaling function, $\tau_{DIP} \simeq 1.33$ and $1/\sigma_{DIP} \simeq 3.5$. The value of τ_{DIP} characterizes the "zigzag" universality
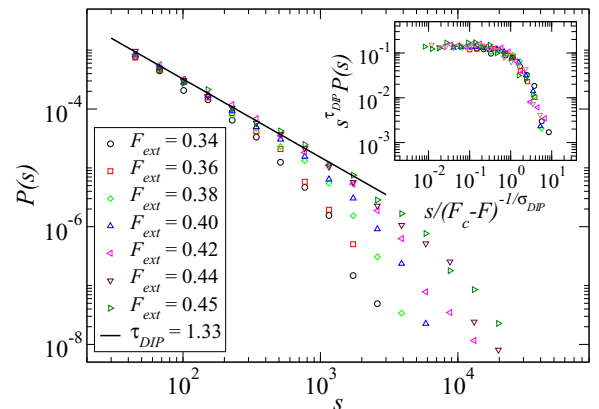

FIG. 4. (Color online) The distribution of avalanche sizes s with $\lambda = 1$, corresponding to the limit dominated by dipolar interactions, for various $F_{ext} \leqslant F_c$. The inset shows a collapse with exponents $\tau_{DIP} = 1.33$ and $1/\sigma_{DIP} = 3.5$.

class dominated by dipolar interactions, and is close to that found for certain other systems with long-range anisotropic interaction kernels, such as models of amorphous plasticity [25]. For larger λ, while large enough avalanches are still dominated by the dipolar interactions, small avalanches start to be governed by the surface tension, and are thus expected to obey the LIM/qEW scaling. Therefore the scaling form in Eq. (6) has to be replaced by a crossover scaling form including two different power laws with the corresponding τ exponents (τ_{LIM} and τ_{DIP}),

$$P(s,s/s_0,s/s_\chi) = s^{-\tau_{\mathrm{LIM}}}\mathcal{G}(s/s_0,s/s_\chi), \qquad (7)$$

where the two-variable scaling function is given by

$$\mathcal{G}(x,y) = \frac{e^{-x}}{(1 + y^{(\tau_{\mathrm{DIP}} - \tau_{\mathrm{LIM}})\kappa})^{1/\kappa}}, \qquad (8)$$

with s_χ a crossover avalanche size separating the two regimes, κ controls the sharpness of the crossover and s_0 is the cut-off avalanche size. The short length scale exponent is expected to be that of the LIM/qEW, $\tau_{\mathrm{LIM}} \simeq 1.11$ [26] and $1/\sigma_{\mathrm{LIM}} = 3.0$ [3].

To estimate the crossover scale L_χ (and the corresponding crossover avalanche size s_χ) above which the dipolar forces will dominate the line tension, we consider the continuum version of Eq. (3) for small deformation of the DW without disorder and external force,

$$\frac{\partial h}{\partial t} = \lambda\frac{\partial^2 h}{\partial x^2} + 4\int\frac{h(x) - h(x')}{|x - x'|^3}dx', \qquad (9)$$

and examine the stability of a flat DW. By writing the two interaction terms in Eq. (9) in terms of their Fourier transforms, $\lambda\frac{\partial^2 h_i}{\partial x^2} = \int dq h_q e^{i2\pi qx}(-4\pi^2\lambda q^2)$ and $4\int dx\frac{h(x)-h(x')}{|x-x'|^3} = 4\int dq e^{i2\pi qx}h_q\int dx'\frac{1-e^{i2\pi q(x'-x)}}{|x-x'|^3}$, one arrives at a stability condition for the mode q, $-4\pi^2\lambda q^2 + I(q) < 0$, where $I(q) \equiv 4\int dr\frac{1-e^{i2\pi qr}}{|r|^3}$. We expand $I(q)$ for small q, such that $I(q) \simeq 8\pi^2\int_1^{1/q} dr(qr)^2/|r|^3 = -8\pi^2 q^2\ln(q)$. Thus, the stability condition becomes $2\ln(q) + \lambda > 0$, which leads to a crossover length

$$L_\chi = e^{\lambda/2}. \qquad (10)$$

The crossover avalanche size is expected to scale as $s_\chi \sim L_\chi^{1+\zeta_\chi}$, where ζ_χ is the roughness exponent of the avalanches at the crossover scale. Thus, also the crossover avalanche size is an exponential in λ,

$$s_\chi = e^{(1+\zeta_\chi)\lambda/2}. \qquad (11)$$

Notice that this form is different from the one employed in Ref. [10].

To test this argument, we simulate the model for various $\lambda \geqslant 1$, and estimate $s_\chi(\lambda)$ by fitting Eq. (7) to the data. We found that Eqs. (7) and (8) with $\kappa = 10$ (corresponding to a sharp crossover), $\tau_{\mathrm{LIM}} = 1.11$ and $\tau_{\mathrm{DIP}} = 1.33$ produce a very good fit; see Fig. 5. Figure 6(a) shows the resulting $s_\chi(\lambda)$ data, which can be well fitted by an exponential, thus confirming the functional form in Eq. (11). Estimating the value of the crossover roughness exponent ζ_χ in Eq. (11) from the exponential fit leads to $(1 + \zeta_\chi)/2 = 1.577$ (Fig. 6), or $\zeta_\chi = 2.15$, somewhat larger than the ζ values measured
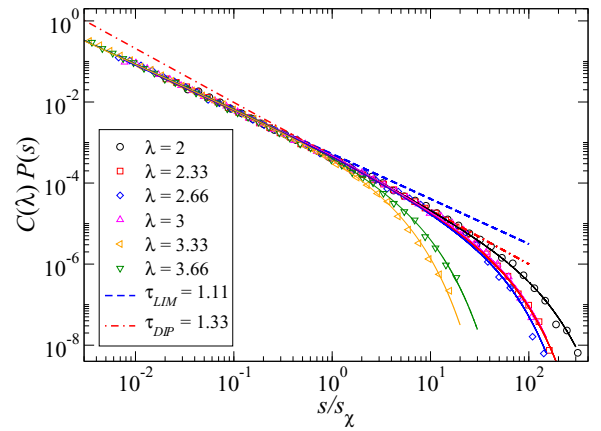

FIG. 5. (Color online) The rescaled avalanche size distributions for various λ, with F slightly below F_c in each case, showing the crossover between the two scaling exponents, $\tau_{\mathrm{LIM}} = 1.11$ (dashed blue line) and $\tau_{\mathrm{DIP}} = 1.33$ (dash-dotted red line). The solid lines are fits of Eq. (7) to the data. The dependence of the crossover avalanche size s_χ on λ resulting from the fits is reported in Fig. 6(a). The factors $C(\lambda)$ are chosen to make the rescaled distributions overlap in the scaling regime.

in Fig. 3. We think this small difference is due to the approximations made in deriving Eq. (11). Figure 5 shows the avalanche size distributions for different λ, with s rescaled with the corresponding $s_\chi(\lambda)$ and $P(s)$ by the factors $C(\lambda)$, chosen to make the different distributions overlap. This procedure reveals a clear crossover scaling, with the exponents $\tau_{\mathrm{LIM}} \simeq 1.11$ and $\tau_{\mathrm{DIP}} \simeq 1.33$ below and above $s/s_\chi = 1$, respectively. Notice also that the crossover is rather sharp, taking place within one order of magnitude in s/s_χ. This is in contrast to the results of Ref. [10], where a large crossover region with a slowly changing effective exponent was found, by using an expression for the crossover avalanche size which is different from the one found here. The crossover can also be seen by fitting a single power law with an exponential cutoff,

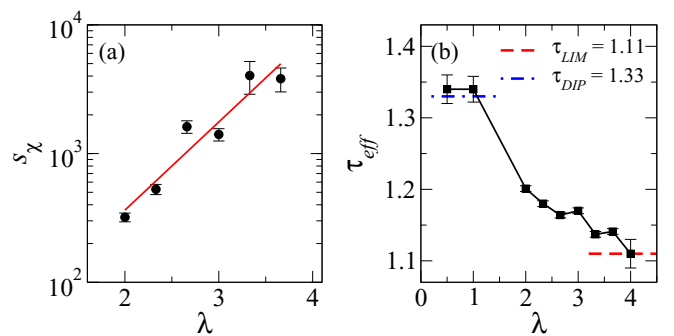$$P(s) = s^{-\tau_{\mathrm{eff}}(\lambda)}\exp\left(-\frac{s}{s_0(\lambda)}\right), \qquad (12)$$

FIG. 6. (Color online) Panel (a) shows the exponential dependence of the crossover avalanche size s_χ on λ. The solid line corresponds to an exponential fit $s_\chi = Ae^{B\lambda}$, with $A = 15.5$ and $B = 1.577$. Panel (b) shows the effective exponent τ_{eff} as obtained by fitting Eq. (12) to the data.

to the data. The resulting effective exponent τ_{eff} as a function of λ is shown in Fig. 6(b), showing again a crossover between the values of $\tau_{\text{LIM}} = 1.11$ and $\tau_{\text{DIP}} = 1.33$.

IV. DISCUSSION

We have presented a theoretical analysis and a numerical model of DW morphology and avalanche dynamics in thin films with in-plane uniaxial anisotropy, giving rise to charged head-to-head (or tail-to-tail) DW's. As a result of the competition between DW surface tension and dipolar interactions, the DW's develop a zigzag structure. The avalanche dynamics displays a sharp crossover between two universality classes, characterized by the exponents $\tau_{\text{LIM}} \simeq 1.11$ and $\tau_{\text{DIP}} \simeq 1.33$, for scales dominated by the line tension and dipolar interactions, respectively. These two scaling regimes are separated by a crossover avalanche size s_χ which exhibits an exponential dependence on $\lambda \sim 1/M_s^2$. It is worth noticing that the dipolar interactions scale as $q^2 \log(q)$ in Fourier space. Hence, in the $q \to 0$ limit, the kernel is similar to a negative surface tension, and it is therefore not possible to infer the dipolar universality class based on simple power counting (as claimed, e.g., in [10]). It would instead be necessary to perform a functional renormalization-group calculation along the lines of Refs. [27–32], taking into account explicitly the nonconvex nature of the interaction kernel, leading to a violation of the no-passing rule usually obeyed by depinning interfaces [21].

[1] G. Durin and S. Zapperi, in *The Science of Hysteresis*, edited by G. Bertotti and I. Mayergoyz (Academic, Amsterdam, 2006), Vol. II, pp. 181–267.

[2] J. P. Sethna, K. A. Dahmen, and C. R. Myers, Nature (London) **410**, 242 (2001).

[3] S. Zapperi, P. Cizeau, G. Durin, and H. E. Stanley, Phys. Rev. B **58**, 6353 (1998).

[4] G. Durin and S. Zapperi, Phys. Rev. Lett. **84**, 4705 (2000).

[5] N. J. Wiegman, Appl. Phys. **12**, 157 (1977).

[6] N. J. Wiegman and R. Stege, Appl. Phys. **16**, 167 (1978).

[7] E. Puppin, Phys. Rev. Lett. **84**, 5415 (2000).

[8] D.-H. Kim, S.-B. Choe, and S.-C. Shin, Phys. Rev. Lett. **90**, 087203 (2003).

[9] L. Santi, F. Bohn, A. D. C. Viegas, G. Durin, A. Magni, R. Bonin, S. Zapperi, and R. L. Sommer, Physica B **384**, 144 (2006).

[10] K.-S. Ryu, H. Akinaga, and S.-C. Shin, Nat. Phys. **3**, 547 (2007).

[11] A. Schwarz, M. Liebmann, U. Kaiser, R. Wiesendanger, T. W. Noh, and D. W. Kim, Phys. Rev. Lett. **92**, 077206 (2004).

[12] M. Liebmann, A. Schwarz, U. Kaiser, R. Wiesendanger, D.-W. Kim, and T.-W. Noh, Phys. Rev. B **71**, 104431 (2005).

[13] S. S. P. Parkin, M. Hayashi, and L. Thomas, Science **320**, 190 (2008).

[14] M. Hayashi, L. Thomas, R. Moriya, C. Rettner, and S. P. Parkin, Science **320**, 209 (2008).

[15] A. Mughal, L. Laurson, G. Durin, and S. Zapperi, IEEE Trans. Magn. **46**, 228 (2010).

[16] B. Cerruti and S. Zapperi, Phys. Rev. B **75**, 064416 (2007).

[17] B. Cerruti and S. Zapperi, J. Stat. Mech. (2006) P08020.

[18] X. Che and H. Suhl, Phys. Rev. Lett. **64**, 1670 (1990).

[19] X. Y. Zhang, H. Suhl, and P. K. George, J. Appl. Phys. **63**, 3257 (1988).

[20] G. Bertotti, *Hysteresis in Magnetism* (Academic, Boston, 1998).

[21] A. A. Middleton, Phys. Rev. Lett. **68**, 670 (1992).

[22] K.-S. Ryu, S.-C. Shin, H. Akinaga, and T. Manago, Appl. Phys. Lett. **88**, 122509 (2006).

[23] E. E. Ferrero, S. Bustingorry, and A. B. Kolton, Phys. Rev. E **87**, 032122 (2013).

[24] See https://github.com/gdurin/pyFitting; using the maximum likelihood method yields comparable results.

[25] M. Talamali, V. Petäjä, D. Vandembroucq, and S. Roux, Phys. Rev. E **84**, 016115 (2011).

[26] A. Rosso, P. Le Doussal, and K. J. Wiese, Phys. Rev. B **80**, 144204 (2009).

[27] T. Nattermann, S. Stepanow, L. H. Tang, and H. Leschhorn, J. Phys. II (France) **2**, 1483 (1992).

[28] O. Narayan and D. S. Fisher, Phys. Rev. B **48**, 7030 (1993).

[29] H. Leschhorn, T. Nattermann, S. Stepanow, and L. H. Tang, Ann. Phys. **6**, 1 (1997).

[30] D. Ertas and M. Kardar, Phys. Rev. E **49**, R2532 (1994).

[31] P. Chauve and T. Giamarchi, and P. Le Doussal, Phys. Rev. B **62**, 6241 (2000).

[32] P. Le Doussal, K. J. Wiese, and P. Chauve, Phys. Rev. B **66**, 174201 (2002).